Received 18 May 2018; | Revised 13 February 2019; | Accepted -

DOI: xxx/xxxx

ARTICLE TYPE

Time-domain Homogenization of Multiturn Windings Based on *RL* Cauer Ladder Networks

Korawich Niyomsatian*[1,2] | Johan Gyselinck[2] | Ruth V. Sabariego[1]

[1]Department of Electrical Engineering, KU Leuven, Campus EnergyVille, 3600 Genk, Belgium

[2]BEAMS Department, Université Libre de Bruxelles, 1050 Brussels, Belgium

Correspondence

*Korawich Niyomsatian, Department of Electrical Engineering, KU Leuven, Campus EnergyVille, 3600 Genk, Belgium. Email: korawich.niyomsatian@kuleuven.be

Present Address

Department of Electrical Engineering, KU Leuven, Campus EnergyVille, 3600 Genk, Belgium

Summary

This paper deals with the synthesis of an *RL* Cauer ladder network to homogenize multiturn windings in time-domain finite element (FE) computations. In frequency domain, the macroscopic model of eddy currents in the winding can be described by frequency-dependent complex impedance and reluctivity for skin and proximity effects respectively. To represent those in time domain, two *RL* Cauer networks are synthesized to match each, with the accuracy depending on the order of the network to be appended. The proposed method yields an improved accuracy as compared to the previous work in which the topology of the ladder network was not well chosen. The results are validated by means of a 2-D axisymmetric inductor with a nonlinear gapped core.

KEYWORDS:
Homogenization of windings, Eddy currents, Time domain simulation, Finite element method

1 | INTRODUCTION

High-frequency operations of electromagnetic devices can incur excessive losses in their windings due to eddy currents. Indeed, when applying high-frequency voltage or current, the current does not flow uniformly, but tends to flow in the layer near the surface of the conductor (the higher the frequency, the thinner the layer).

In finite element (FE) modeling, the conventional brute-force approach requires fine mesh in each turn of a winding to accurately capture this phenomenon, which can lead to an extremely high computational cost, particularly in three-dimensional (3-D) models. Homogenization techniques that refrain from the fine discretization of the winding are indispensable in FE models. The homogenization consists in transforming a heterogeneous material like a winding region (consisting of conductors, insulation and air) into a homogeneous material, the mesh of which can be significantly coarser.

If the supply is sinusoidal and the system is linear, frequency-domain homogenization methods provide a steady-state solution, e.g. techniques in Gyselinck (2005)[1], Meunier (2008)[2]. Therein, the eddy-current effect in the winding is macroscopically modeled by means of a complex impedance (or admittance) and a complex reluctivity (or permeability), which are extracted from solving a cell problem. Their formulas have also been proposed based on the fit of FE solutions to the cell problem[3,4,5] and based on the effective medium theory[6]. The winding homogenization approach is also extended within a harmonic-balance FE method allowing for non-sinusoidal supplies and nonlinearities by means of multi-harmonic impedance and reluctivity[7] (a complex value per harmonic in the system). However, in the case of transient analysis (linear or nonlinear systems), the time-domain simulation is necessary.

One straightforward way to model frequency-dependent behavior in time-domain simulations is to employ an *RL* ladder network (e.g. Figure 1), of which the order determines the modeling accuracy[8]. To incorporate the homogenization of the winding in time-domain FE computation, Gyselinck (2007)[9] and Sabariego (2008)[10] synthesized an *RL* ladder network in Figure 1 b. The system matrices corresponding to this network were fitted based on the frequency-domain complex impedance and reluctivity[1] using a constrained Nelder-Mead simplex optimization algorithm. A similar method has been conducted for soft magnetic composites[11]. Sato (2016)[12] applied a Padé approximation via a Lanczos process to produce a reduced transfer function of an inductor model. The resulting Foster network allows to account for the eddy-current effects in the winding. Kameari (2018)[13] proposed characterizing a nonlinear inductor with a Cauer ladder network, which was synthesized iteratively. The result of the synthesis also provides the electric and magnetic fields which subsequently are the sources of its FE model. The total solution is achieved by superposition.

(a) Cauer network

(b) Network considered in the previous study [10]

FIGURE 1 Examples of 3rd-order RL ladder networks.

In this paper, we propose an improved method of winding homogenization for time-domain FE computation as compared to the research by Gyselinck (2007) [9] and Sabariego (2008) [10]. An RL Cauer ladder network in Figure 1 a is synthesized based on the estimation of a transfer function from precomputed frequency-dependent complex impedance (skin effect) and reluctivity (proximity effect) [1]. The employed estimation algorithm is vector fitting (VF) based, which are popular identification methods through iterative applications of least-square problems [14,15]. The method has been successfully applied in transient simulations of multiturn transformers [16,17]. Accordingly, the component values are determined by the simple Euclidean algorithm for polynomial division. Effects of the order of the synthesized networks on the modeling accuracy are also investigated. Compared to the work by Kameari (2018) [13], our method allows the straightforward coupling of the FE model with the RL Cauer ladder network via the global currents and voltages for the skin-effect network, and via the local magnetic flux density in the winding for the proximity-effect network. For validation, we consider a 2-D model of an axisymmetric inductor model with a nonlinear gapped core, for which a conventional brute-force model provides an accurate reference solution.

In this work, we adopt the following assumptions:

- We restrict our study to magneto-quasi-static problems with sufficiently low working frequency, so that the displacement currents and ensuing capacitive effects (winding capacitance) can be disregarded. As a rule of thumb, the highest relevant frequency should be below one third of the resonant frequency, ensuring that the capacitive current is at least one order of magnitude lower than the inductive current [18]. Violating this rule can potentially lead to inaccurate transient simulations, e.g. when modeling lightning strikes at transformers where capacitive currents are significant.

- The winding of interest is relatively orderly wound, which is common practice in electrical machines and power magnetic devices. Note that such a neat structure allows to estimate the static winding parasitic capacitance and achieve an accurate transient response [19]. This capacitance value, required to estimate the resonance frequency, can be determined either from the winding and core geometry and material characteristics (see e.g. Dalessandro (2007) [20]) or from electrostatics finite-element models (see e.g. De Grève (2013) [21]).

2 | MACROSCOPIC MODEL OF EDDY CURRENTS IN MULTITURN WINDINGS

In the frequency domain with frequency f or angular frequency (pulsation) $\omega = 2\pi f$, the macroscopic modeling of eddy currents in the winding (conductor radius r, fill factor λ, length l and DC resistance R_dc) can be done through the phasor and complex-quantities representation with $\mathrm{j} = \sqrt{-1}$ [1]. Given, the conductivity of the conductor σ, the permeability of the conductor μ_0 (or the reluctivity $\nu_0 = 1/\mu_0$), the skin effect can be represented by the frequency-dependent complex impedance

$$\underline{Z}_\mathrm{skin}(\mathrm{j}\omega) = p_\mathrm{I}(\omega) R_\mathrm{dc} + \mathrm{j}\omega q_\mathrm{I}(\omega) \frac{\mu_0 l}{8\pi\lambda}\,, \tag{1}$$

through the frequency-dependent coefficients p_I and q_I, whereas the proximity effect can be represented by the frequency-dependent complex reluctivity (the reciprocal of the complex permeability)

$$\underline{\nu}_\mathrm{prox}(\mathrm{j}\omega) = q_\mathrm{B}(\omega)\nu_0 + \mathrm{j}\omega p_\mathrm{B}(\omega) \frac{\lambda\sigma r^2}{4}\,, \tag{2}$$

through the frequency-dependent coefficients p_B and q_B.

Since the imaginary parts of these two complex quantities are proportional to the angular frequency ω for sufficiently low angular frequency, they can be approximated to the frequency-domain behavior of an RL network, which can also be described by a system of the k first-order ordinary differential equations (ODEs) in time domain with large enough k. For skin effect, it is straightforward to relate the instantaneous voltage and current, which are the winding global quantities, as follows:

$$\underline{\mathbf{v}}(\mathrm{j}\omega) = \mathbf{R}\underline{\mathbf{i}}(\mathrm{j}\omega) + \mathrm{j}\omega\mathbf{L}\underline{\mathbf{i}}(\mathrm{j}\omega) \Longleftrightarrow \mathbf{v}(t) = \mathbf{R}\mathbf{i}(t) + \mathbf{L}\frac{\mathrm{d}}{\mathrm{d}t}\mathbf{i}(t)\,, \tag{3}$$

where $\underline{\mathbf{v}}(\mathrm{j}\omega)$ and $\underline{\mathbf{i}}(\mathrm{j}\omega)$ are the k-element column vectors of complex-valued voltage and current phasors in the network respectively, $\mathbf{v}(t)$ and $\mathbf{i}(t)$ are the k-element column vectors of instantaneous voltages and currents in the network, and $\mathbf{R}$ and $\mathbf{L}$ are the $k \times k$ constant real symmetric matrices associated with the resistive and inductive elements in the network. In general, the network can be described in time domain by the terminal voltage $v(t)$, together with the terminal current $i(t)$ and $k-1$ auxiliary currents in the network $i_2(t), \ldots i_k(t)$. The column vectors $\mathbf{v}(t)$ and $\mathbf{i}(t)$ associated with Figure 1 are $[\, v(t) \;\; 0 \;\; \cdots \;\; 0 \,]^T$ and

$[\, i(t)\ \ i_2(t)\ \ \cdots\ \ i_k(t)\,]^T$ respectively. In addition, the magnetic energy w_{skin} and the joule losses p_{skin} due to skin effect can be computed from the instantaneous power $\mathbf{v}^T(t)\mathbf{i}(t)$ based on (3) by

$$w_{\text{skin}}(t) = \int \left(\frac{\mathrm{d}}{\mathrm{d}t}\mathbf{i}^T(t)\right)\mathbf{L}\mathbf{i}(t)\,\mathrm{d}t = \int \frac{\mathrm{d}}{\mathrm{d}t}\left(\frac{1}{2}\mathbf{i}^T(t)\mathbf{L}\mathbf{i}(t)\right)\mathrm{d}t = \frac{1}{2}\mathbf{i}^T(t)\mathbf{L}\mathbf{i}(t)\,, \tag{4}$$

$$p_{\text{skin}}(t) = \mathbf{i}^T(t)\mathbf{R}\mathbf{i}(t)\,. \tag{5}$$

Although there is no physical circuit governing the relation between the local instantaneous magnetic field intensity $h(t)$ and magnetic flux density $b(t)$, the proximity-effect reluctivity can be analogously expressed through the following relation

$$\underline{\mathbf{h}}(\mathrm{j}\omega) = \mathfrak{R}\underline{\mathbf{b}}(\mathrm{j}\omega) + \mathrm{j}\omega\mathfrak{L}\underline{\mathbf{b}}(\mathrm{j}\omega) \Longleftrightarrow \mathbf{h}(t) = \mathfrak{R}\mathbf{b}(t) + \mathfrak{L}\frac{\mathrm{d}}{\mathrm{d}t}\mathbf{b}(t)\,, \tag{6}$$

where $\underline{\mathbf{h}}(\mathrm{j}\omega)$ and $\underline{\mathbf{b}}(\mathrm{j}\omega)$ are the k-element column vectors of complex-valued magnetic field intensity and magnetic flux density phasors respectively, $\mathbf{h}(t)$ and $\mathbf{b}(t)$ are the k-element column vectors of instantaneous magnetic field intensity and magnetic flux density, and $\mathfrak{R}$ and $\mathfrak{L}$ are $k \times k$ constant real symmetric matrices. Therefore, the column vectors $\mathbf{h}(t)$ and $\mathbf{b}(t)$ can be $[\, h(t)\ \ 0\ \ \cdots\ \ 0\,]^T$ and $[\, b(t)\ \ b_2(t)\ \ \cdots\ \ b_k(t)\,]^T$ respectively, where $b_2(t), \ldots b_k(t)$ are $k-1$ auxiliary components of magnetic flux density.

Based on the local relation in (6), we can compute the instantaneous magnetic energy w_{prox} and joule losses p_{prox} due to proximity effect in the winding region Ω_{winding} from [10]

$$w_{\text{prox}}(t) = \int\limits_{\Omega_{\text{winding}}} \frac{1}{2}\mathbf{b}^T(t)\mathfrak{R}\mathbf{b}(t)\,\mathrm{d}\Omega\,, \tag{7}$$

$$p_{\text{prox}}(t) = \int\limits_{\Omega_{\text{winding}}} \frac{1}{2}\left(\frac{\mathrm{d}}{\mathrm{d}t}\mathbf{b}^T(t)\right)\mathfrak{L}\frac{\mathrm{d}}{\mathrm{d}t}\mathbf{b}(t)\,\mathrm{d}\Omega\,. \tag{8}$$

Therefore, the total magnetic energy in the winding region w_{winding} and the total winding losses p_{winding} can be calculated from

$$w_{\text{winding}}(t) = w_{\text{skin}}(t) + w_{\text{prox}}(t)\,, \tag{9}$$

$$p_{\text{winding}}(t) = p_{\text{skin}}(t) + p_{\text{prox}}(t)\,. \tag{10}$$

3 | *RL* LADDER NETWORKS FOR TIME-DOMAIN SIMULATION

An RL ladder network is a useful tool to model frequency-dependent behavior. The order k of the network can be chosen to obtain a desired accuracy of the model over a desired range of frequency (cf. Figure 1 for some examples of 3rd-order ladder networks). One of the most useful topologies of RL ladder networks is a Cauer network[1] (Figure 1 a), of which the synthesis procedure has been well established [23]. In the s-domain (where $s = \mathrm{j}\omega$), such networks can be synthesized to have the driving-point admittance $\underline{Y}(s) = 1/\underline{Z}(s)$ that perfectly matches any rational, causal and stable transfer function provided that

$$\left|\underline{Z}(\mathrm{j}\infty)\right| > \left|\underline{Z}(\mathrm{j}0)\right| = R_{\text{dc}}\,. \tag{11}$$

The RL component values in the network can be found by a continued fraction expansion of the driving-point impedance $\underline{Z}(s)$, e.g. the case of a 3rd-order RL ladder network is

$$\underline{Z}(s) = R_1 + \cfrac{1}{\cfrac{1}{sL_1} + \cfrac{1}{R_2 + \cfrac{1}{\cfrac{1}{sL_2} + \cfrac{1}{R_3 + \cfrac{1}{sL_3}}}}}. \tag{12}$$

This can be done easily by the simple Euclidean algorithm for polynomial division in numerical analysis software, e.g. command `deconv` in MATLAB. Moreover, if the transfer function is scaled to the new frequency ω_{new} (frequency scaling), the synthesized network can be simply modified by scaling the inductance values as follows:

$$\omega_{\text{new}} = k\omega_{\text{old}} \Longrightarrow L_{\text{new}} = L_{\text{old}}/k. \tag{13}$$

[1]The other topology of Cauer network can be derived by swapping the positions of inductors and resistors, resulting in a network with series inductors and shunt resistors. This topology is preferred to model the saturation of the magnetic core [22]. However, to represent a linear subsystem like the winding in this work, both topologies can be used, so the topology in Figure 1 a is selected.

On the other hand, if the transfer function is scaled to the new impedance level $\left|\underline{Z}_{\mathrm{new}}\right|$ (impedance scaling), the synthesized network can be simply modified by scaling the inductance and the resistance values as follows:

$$\left|\underline{Z}_{\mathrm{new}}\right| = \alpha \left|\underline{Z}_{\mathrm{old}}\right| \Longrightarrow L_{\mathrm{new}} = \alpha L_{\mathrm{old}} \text{ and } R_{\mathrm{new}} = \alpha R_{\mathrm{old}}. \tag{14}$$

From (3), a k^{th}-order RL Cauer ladder network in Figure 1 a can be described in time domain by the diagonal matrix $\mathbf{R}$ and the symmetric tridiagonal matrix $\mathbf{L}$ reading

$$\mathbf{R} = \begin{bmatrix} R_1 & 0 & \dots & 0 \\ 0 & R_2 & \dots & 0 \\ \vdots & \vdots & \ddots & 0 \\ 0 & 0 & 0 & R_k \end{bmatrix}, \quad \mathbf{L} = \begin{bmatrix} L_1 & -L_1 & \dots & 0 \\ -L_1 & L_1 + L_2 & \dots & 0 \\ \vdots & \vdots & \ddots & -L_{k-1} \\ 0 & 0 & -L_{k-1} & L_{k-1} + L_k \end{bmatrix}. \tag{15}$$

Analogously, the matrices $\mathfrak{R}$ and $\mathfrak{L}$ in (6) are diagonal and symmetric tridiagonal respectively and can be written in the same way.

3.1 | Synthesis of RL ladder networks

The synthesis procedure can be summarized as follows:

1. Obtain the normalized frequency responses of the complex impedance $\underline{Z}_{\mathrm{n,skin}}(\mathrm{j}\omega_{\mathrm{n}})$ and the complex reluctivity $\underline{\nu}_{\mathrm{n,prox}}(\mathrm{j}\omega_{\mathrm{n}})$ of the winding, where $\left|\underline{Z}_{\mathrm{n,skin}}(\mathrm{j}0)\right| = \left|\underline{\nu}_{\mathrm{n,skin}}(\mathrm{j}0)\right| = 1$. They can be obtained by the empirical formulas[3,4,5,6] or by solving a representative cell problem[1]. In this work, we solved the cell problem with the FE method in open-source software Gmsh/GetDP[24,25] for each normalized frequency ω_{n}

$$\omega_{\mathrm{n}} = \left(\frac{r}{\delta}\right)^2 = \overbrace{\left(\frac{\sigma\mu_0 r^2}{2}\right)}^{p_{\mathrm{n}}}\omega = p_{\mathrm{n}}\omega \tag{16}$$

   where $\delta = 1/\sqrt{(\sigma\pi\mu_0 f)}$ is the skin-depth of the conductor.

2. Estimate a corresponding rational transfer function. In this work, we fitted $\underline{Y}_{\mathrm{n,skin}}(\mathrm{j}\omega) = 1/\underline{Z}_{\mathrm{n,skin}}(\mathrm{j}\omega)$ and $\underline{\mu}_{\mathrm{n,prox}}(\mathrm{j}\omega) = 1/\underline{\nu}_{\mathrm{n,prox}}(\mathrm{j}\omega)$ instead because they are bounded. We used the function `tfest` based on the vector fitting algorithm[14] from the system identification toolbox in MATLAB with the condition that the number of poles is higher than the number of zeros by one to satisfy (11).

3. Synthesize a corresponding RL Cauer ladder network based on (12).

4. Scale the inductance value $L \rightarrow p_{\mathrm{n}}L$.

5. Scale both the resistance and inductance values with the DC values, i.e. R_{dc} and ν_0 for complex impedance and complex reluctivity respectively.

3.2 | Synthesis results

To investigate the effect of the order of the synthesized ladder network on modeling accuracy, the Cauer ladder networks of order from 1 to 4 are synthesized to match the FE solution to a cell problem of square-packed windings[1] with fill factor $\lambda = 0.65$ over 40 logarithmically spaced frequencies in the range of $\omega_{\mathrm{n}} \in [0, 100]$. The results from the previous work[10] with the ladder network in Figure 1 b are also included for comparison. Apart from different network topologies (cf. Figure 1 a&b), in the previous study, the matrices $\mathbf{R}$ in (3) and $\mathfrak{R}$ in (6) are fixed to be the identity matrices (all series resistors in Figure 1 b have the same value.), and the estimation algorithm relies on a constrained Nelder-Mead simplex optimization algorithm of the functions `fminsearchbnd` to ensure only finite positive-valued elements (physically realizable). Herein, the normalized root mean square (RMS) error is a metric for comparing the goodness of approximations $\hat{\underline{H}}$ to a complex-valued N_{data}-element data set $\underline{H}$, reading

$$\text{Normalized RMS Error, } \epsilon = \sqrt{\frac{1}{N_{\mathrm{data}}}\sum_{i}^{N_{\mathrm{data}}}\left|\frac{\hat{\underline{H}}_i - \underline{H}_i}{\underline{H}_i}\right|^2}. \tag{17}$$

For the skin-effect impedance, the results in this paper and in the previous work are comparable (Figure 2 a). The increase in order improves the accuracy of the estimate. The phase response obtained from the synthesized ladder network deviates from the reference solution at high frequencies despite using the 4^{th}-order network. Still, in multiturn winding applications, the proximity effect is dominant so this does not cause significant errors[1]. The corresponding synthesized 4^{th}-order network is displayed in Figure 3 . The first resistor next to the terminal of the synthesized network has the value of $R_{\mathrm{dc}} = 0.187\,\Omega$, which corresponds to the asymptotic low-frequency behavior of the network. In other words, increasing the order of the network augments the network with additional ladder elements to improve the accuracy at high frequencies.

For the proximity-effect reluctivity, the results of the synthesis in this work are in good agreement with the reference solution (Figure 2 b). When the order of the network is higher than 2, the error ϵ decreases 10 times per one-order increment. Furthermore, compared to the results based on the previous work, the

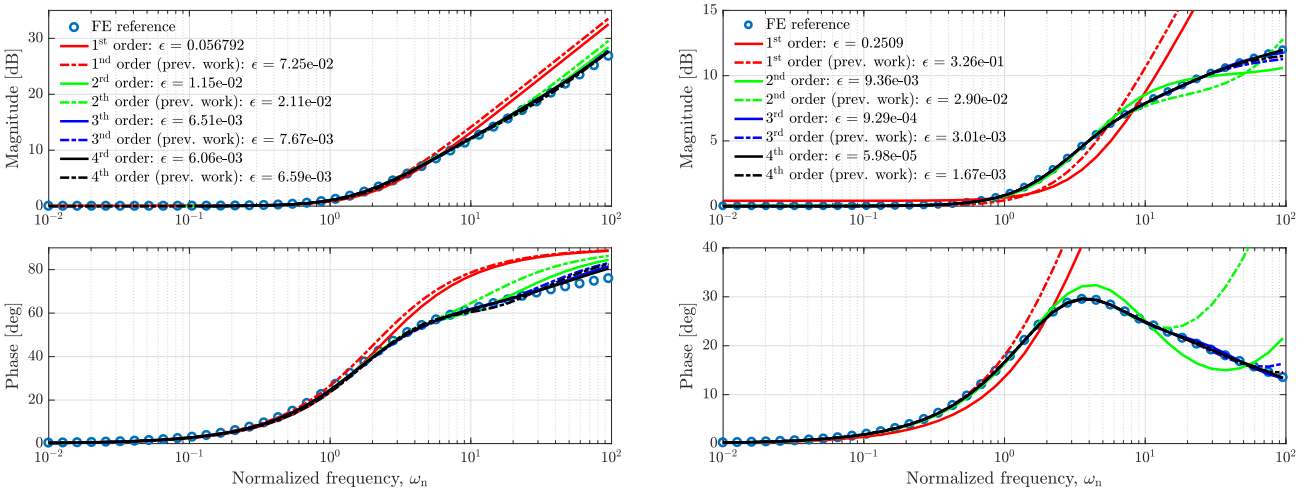

(a) Skin-effect impedance $\underline{Z}_{\text{skin}}$ **(b)** Proximity-effect reluctivity $\underline{\nu}_{\text{prox}}$

FIGURE 2 Fitted frequency-dependent skin-effect complex impedance $\underline{Z}_{\text{skin}}$ (a) and reluctivity $\underline{\nu}_{\text{prox}}$ (b) of fill factor $\lambda = 0.65$ based on the Cauer ladder networks of different orders and their normalized RMS errors compared to the reference solutions from the FE method.

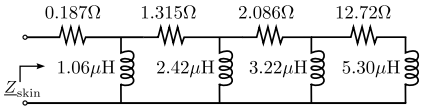

FIGURE 3 Synthesized 4th-order RL Cauer ladder network to represent the skin-effect impedance $\underline{Z}_{\text{skin}}$.

error of the approximation obtained in this paper is 100 times less than the one of the previous work. The corresponding system of differential equations of order 4 is as follows:

$$\begin{bmatrix} h(t) \\ 0 \\ 0 \\ 0 \end{bmatrix} = \nu_0 \begin{bmatrix} 1 & 0 & 0 & 0 \\ 0 & 1.91 & 0 & 0 \\ 0 & 0 & 1.081 & 0 \\ 0 & 0 & 0 & 0.671 \end{bmatrix} \begin{bmatrix} b(t) \\ b_2(t) \\ b_3(t) \\ b_4(t) \end{bmatrix} + \frac{\sigma r^2}{2} \begin{bmatrix} 0.325 & -0.325 & 0 & 0 \\ -0.325 & 0.369 & -0.044 & 0 \\ 0 & -0.044 & 0.0533 & -0.0089 \\ 0 & 0 & -0.0089 & 0.0106 \end{bmatrix} \frac{\mathrm{d}}{\mathrm{d}t} \begin{bmatrix} b(t) \\ b_2(t) \\ b_3(t) \\ b_4(t) \end{bmatrix}. \tag{18}$$

The resultant matrix $\mathfrak{R}$ here is not the identity matrix as assumed in the previous work [10], which indicates the cause of mismatch of the estimate in Figure 2 b.

From Figure 2 , the results suggest that the order of the synthesized RL ladder network should be at least 3 to ensure good accuracy of the modeling for this wide range of frequencies and fill factor $\lambda = 0.65$.

4 | HOMOGENIZATION OF WINDINGS IN FE MODELS

As an application example, a 2-D model of an axisymmetric inductor with a nonlinear gapped core in Figure 4 a is considered. The winding region contains uniformly distributed $N = 120$ round conductors with radius $r = 0.56\,\text{mm}$, connected in series. This is associated with fill factor $\lambda = 0.65$, yielding $R_{\text{dc}} = 0.187\,\Omega$. This obviously requires fine mesh in the winding region, whereas the mesh is much coarser in its homogenized counterpart (Figure 4 b). The winding homogenization was carried out with the order of ladder network $k = 4$ for both skin- and proximity effects. For comparison, the homogenized model based on the previous work is also considered.

To incorporate the homogenized winding based on the synthesized networks into an FE model, the skin-effect impedance and the proximity-effect reluctivity are treated separately. For the former, the electrical circuit equation of its RL Cauer ladder network (Figure 3) is straightforwardly defined as a constraint of the global quantities [2]: voltage $v(t)$ and current $i(t)$. On the other hand, for the proximity-effect reluctivity, which involves local field quantities and does not have the physical meaning of an electrical circuit, the system of 4 first-order differential equations in (18) is synthesized instead to relate the instantaneous local magnetic field intensity $h(t)$ and magnetic flux density $b(t)$ in the winding region Ω_{winding}. This system of differential equations is coupled into the finite element formulation with the additional unknown vector fields $\{b_2, b_3, b_4\}$ in (18) being introduced in the winding region Ω_{winding}. The detailed implementation and its weak FE formulation can be found in Gyselinck (2005) [1] for 2-D models and in Sabariego (2008) [10] for 3-D models. Note that an alternative strategy would

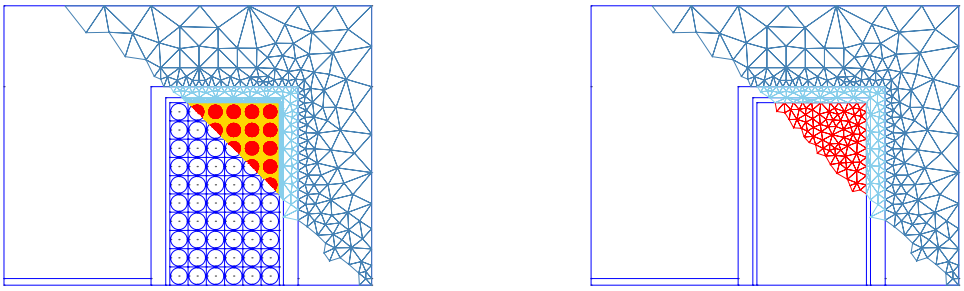

(a) Fine model **(b)** Homogenized model

FIGURE 4 2-D model of an axisymmetric inductor with a nonlinear gapped core

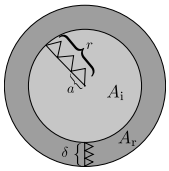

FIGURE 5 Drawing of a simplified round conductor with equilateral triangular elements. For eddy-current computation, the outer part A_r where the current tends to flow requires a fine mesh, whereas the inner part A_i has a coarser mesh.

consist in coupling the skin-effect Cauer ladder network in the finite element formulation via the local current density and auxiliary unknowns in the winding region. However, this would have a detrimental effect on the computational cost while not improving the accuracy. In practice, we opt for the more convenient and natural approach of inserting the skin-effect Cauer network in the electrical circuit[2].

4.1 | Analysis of Computational Costs

Since this winding homogenization method requires inclusion of some additional auxiliary basis functions in the winding region, this causes extra unknowns in the whole model. For the sake of simplicity, we perform this analysis in 2-D and for a triangular discretization. An analogous analysis could be performed in 3-D with e.g. a tetrahedral mesh. To preliminarily prove the usefulness of this homogenization method, the number of resulting triangular elements n_{homog} is compared to the one of a brute-force fine model n_{fine}. The comparison is conservative to show the extreme case where the homogenized model could possibly need more unknowns than the fine model. For simplicity, we assume all the elements in the mesh are equilateral triangles, and the mesh parts elsewhere (core, air gap, etc.) in both homogenized and fine models are identical. We will compare the resulting number of triangular elements in the winding region with fill factor λ.

In the fine model (e.g. Figure 4 a), a conductor is explicitly modeled as shown in Figure 5 ; each disk represents a cross section of a round conductor with radius r, divided into two areas: an annular ring with thickness δ yielding area A_r and an inner circle with radius $r-\delta$ yielding area A_i. Due to the eddy-current phenomenon, the current tends to flow through the former area rather than through the latter area. As a rule of thumb, the characteristic length of a triangular element in this annular ring should be at least $1/3$ of the skin depth δ to accurately capture the eddy-current phenomenon.

In contrast, in the homogenized model, the winding region is modeled by a homogeneous rectangular region, in which the mesh is uniformly generated. Due to additional basis functions, the number of unknowns is proportional to the order of the ladder network $k \geq 1$. For conservative comparison, we choose the side length of an element to be a, which is equal to the side length of the element in the air and insulation of the fine model.

To compare the number of triangular elements of both models, we consider the relative number of the one of the brute-force fine model to the one of the homogenized model $\kappa = n_{\text{fine}}/n_{\text{homog}}$. In other words, the larger κ is, the more advantageous the homogenized model becomes. According to Appendix, the ratio κ reads

$$\kappa = \frac{n_{\text{fine}}}{n_{\text{homog}}} = \frac{\left(1 + \left(\frac{A_i}{A_r} - 1\right)\lambda\right)\frac{A_r}{A_i} + 1}{k\left(\frac{A_r}{A_i} + 1\right)}, \tag{19}$$

TABLE 1 Different mesh sizes and their corresponding results of the homogenized model compared to the fine model

mesh size [m]	no. of unknowns	error of computed magnetic energy, $\epsilon_{W_{\text{winding}}}$	error of computed winding losses, $\epsilon_{P_{\text{winding}}}$
$2r$	2 497	1.33×10^{-3}	1.75×10^{-3}
r	8 341	1.08×10^{-3}	1.83×10^{-3}
$r/2$	30 659	1.04×10^{-3}	1.82×10^{-3}
fine model	28 768	—	—

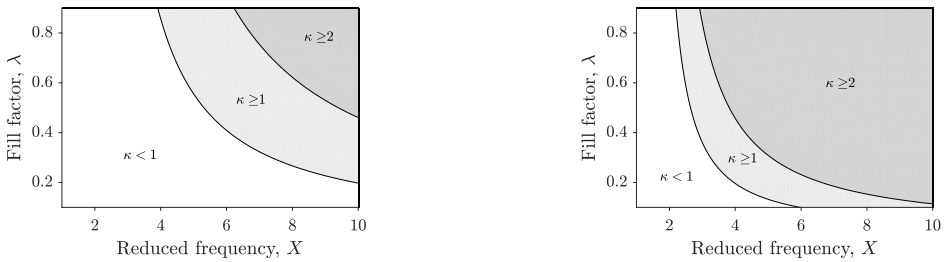

(a) $m = \dfrac{a}{r-\delta} = \dfrac{1}{3}$ **(b)** $m = \dfrac{a}{r-\delta} = \dfrac{2}{3}$

FIGURE 6 The relative number of unknowns of the brute-force fine model with respect to the homogenized model $\kappa = n_{\text{fine}}/n_{\text{homo}}$ as function of the fill factor of the winding region λ and the reduced frequency $X = r/\delta$, where $X \geq 1$ for the case of significant eddy-current effect. The homogenized model is implemented with the 4$^{\text{th}}$-order ladder network ($k = 4$).

where $\dfrac{\Delta_{\text{i}}}{\Delta_{\text{r}}}$ is the ratio of the mesh size around the skin layer to the mesh size in the inner layer of a conductor and $\dfrac{A_{\text{r}}}{A_{\text{i}}}$ is the ratio of the area of the skin part to the area of the inner part of a conductor (Figure 5). These two ratios can be simply written in terms of the reduced frequency [1] $X = r/\delta$ as follows

$$\frac{\Delta_{\text{i}}}{\Delta_{\text{r}}} = \left(\frac{3a}{\delta}\right)^2 = \left(3\frac{a}{r-\delta}\left(\frac{r}{\delta}-1\right)\right)^2 = (3m\,(X-1))^2 \tag{20}$$

with $m = a/(r-\delta)$ indicating the relative mesh size in the inner part of the conductor, and

$$\frac{A_{\text{r}}}{A_{\text{i}}} = \frac{\pi\left(r^2-(r-\delta)^2\right)}{\pi\,(r-\delta)^2} = \frac{2X-1}{(X-1)^2}\,. \tag{21}$$

According to (20) and (21), κ in (19) depends only on the fill factor λ, the reduced frequency $X = r/\delta$ and the order of the ladder network k.

Figure 6 displays κ for two cases of $m = 1/3, 2/3$, using the 4$^{\text{th}}$-order ladder network corresponding to the best accuracy as shown in Section 3.2. From this conservative comparison, if m or the relative mesh size in the inner part becomes larger (larger a), the benefit of the homogenized model becomes clearer for the same reduced frequency X and fill factor λ. The benefit is also noticeable at high frequencies and high fill factors despite additional unknowns from the homogenization method.

Nevertheless, the benefit is not clear at low frequencies and low fill factors in this comparison due mainly to our conservative assumption about the mesh size of the homogenized model. In practice, the side length or characteristic length of the elements in the winding region of the homogenized model can be greater than a, while still yielding high accuracy. To confirm this, we solve the FE homogenized model in Figure 4 with different mesh sizes at $k = 4$ and imposed sinusoidal voltage with frequency of 15 kHz ($X = 1.06$), where $\kappa \leq 1$ in Figure 6 . The computed magnetic energy w_{winding} and winding losses p_{winding} are compared with those from the fine model by normalized RMS errors. According to Table 1 , choosing the side length equal to the conductor diameter $2r$ and to the conductor radius r yields κ around 12 and 3.6 respectively while the accuracy still is acceptable (normalized RMS error of 1.33×10^{-3} and 1.08×10^{-3} respectively for w_{winding} and 1.75×10^{-3} and 1.83×10^{-3} respectively for p_{winding}). However, if the mesh size is finer ($r/2$), the number of unknowns becomes larger than the fine model ($\kappa \leq 1$), but the accuracy does not improve. In practice, this emphasizes the benefit of the homogenized model to yield less number of unknowns while still achieving acceptable accuracy.

4.2 | Sparsity of system matrices

In time domain, after spatial discretization of the models in Figure 4 with the characteristic equal to the conductor radius r and $k = 4$, we obtain the following system of differential equations

$$\mathbf{M}\frac{\mathrm{d}}{\mathrm{d}t}\mathbf{x} + \mathbf{K}\mathbf{x} = \mathbf{u}\,, \tag{22}$$

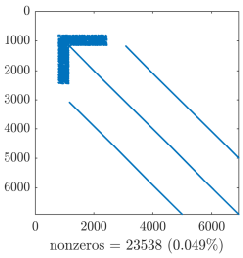

(a) Homogenized model with $k = 4$ (no. of unknowns: 6 901)

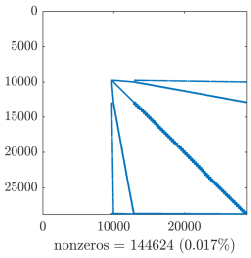

(b) Fine model (no. of unknowns: 28 766)

FIGURE 7 Sparsity pattern of the mass matrix $\mathbf{M}$ ($\lambda = 0.65$ and $X = 1.74$).

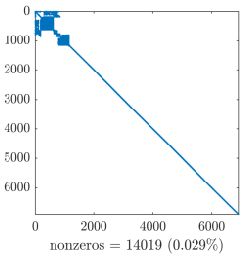

(a) Homogenized model with $k = 4$ (no. of unknown is 6 901)

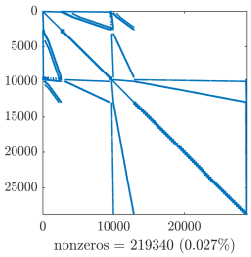

(b) Fine model (no. of unknown is 28 766)

FIGURE 8 Sparsity pattern of the stiffness matrix $\mathbf{K}$ ($\lambda = 0.65$ and $X = 1.74$).

where $\mathbf{x}$ is the solution vector to the FE problem, $\mathbf{u}$ is the imposed source vector for the FE problem, and $\mathbf{M}$ and $\mathbf{K}$ are the mass and stiffness matrices respectively. These matrices in both homogenized and fine models are sparse (Figures 7 and 8). Moreover, the mass and stiffness matrices of the homogenized model have structures of band matrices, which can be more easily treated. Clearly, the added circuit-coupling constraint and the additional auxiliary vector fields due to the skin-effect and proximity-effect homogenization of winding does not corrupt the sparsity of the matrices. Moreover, the number of unknowns in the homogenized model significantly reduces to 6 901 (4 times less than 28 766 unknowns in the fine model).

4.3 | Time-domain FE results

Based on the same mesh generated in the previous section, time-stepping simulations of the homogenized and fine models are conducted with time step $\Delta t = T/100$ by imposing square-wave voltage with fundamental frequency $f = 40\,\text{kHz}$ ($X = 1.74$) in Figure 9 .

The terminal current obtained from the homogenized model is triangular with the average error of only 3×10^{-5} relative to the current peak value, while the one of the homogenized model based on the previous work yields the error of 10^{-4} (Figure 9). Furthermore, the comparison of the total magnetic energy in the winding region w_{winding} (Figure 10) and total winding losses p_{winding} (Figure 11) are made for each order of the synthesized ladder network as well as the results from the homogenized model of the previous work. The improvements of the accuracy of both w_{winding} and p_{winding} can be clearly seen when using the higher-order synthesized networks, particularly between using 1$^{\text{st}}$-order and the 2$^{\text{nd}}$-order synthesized networks. Compared to the results from the previous work, the winding losses from this work are more accurate while the winding magnetic energy is comparable.

Note that the capacitance of the winding of interest in Figure 4 amounts to $C_{\text{eq}} = 12.77\,\text{pF}$ based on Dalessandro(2007)[20]. With the inductance of $L_{\text{eq}} = 2.41\,\text{mH}$, the estimated self resonant frequency[20] is 912 kHz, which is roughly 25 times the switching frequency of the voltage. Therefore, in the considered application, the effects of parasitic capacitance and capacitive currents are substantially insignificant during the transient. Alternatively to full-wave FE computations, one can directly integrate the estimated winding capacitance in the electrical circuit constraint of global winding voltage and current in parallel with the device at the terminal[18], or use a dual formulation coupling magnetodynamics and electrostatics formulations[26].

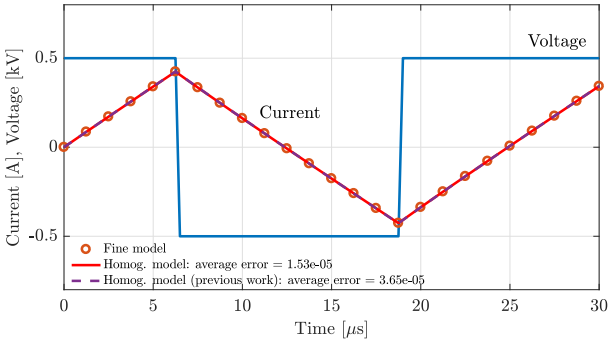

FIGURE 9 Imposed voltage and current simulated from the fine model and the homogenized model.

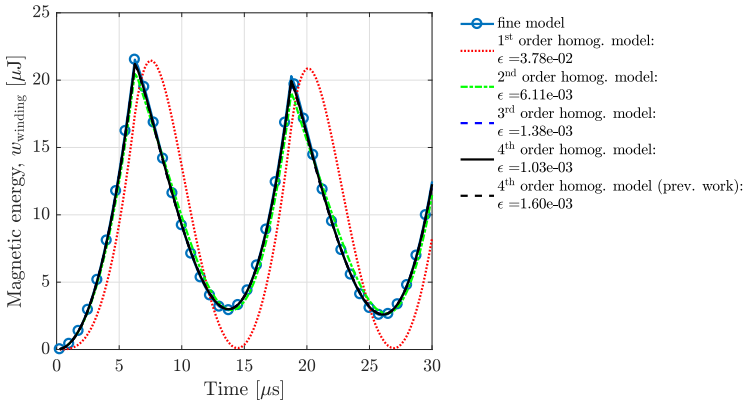

FIGURE 10 Magnetic energy in the winding region computed from the fine model and the homogenized model with synthesized networks of different orders, and their normalized RMS errors.

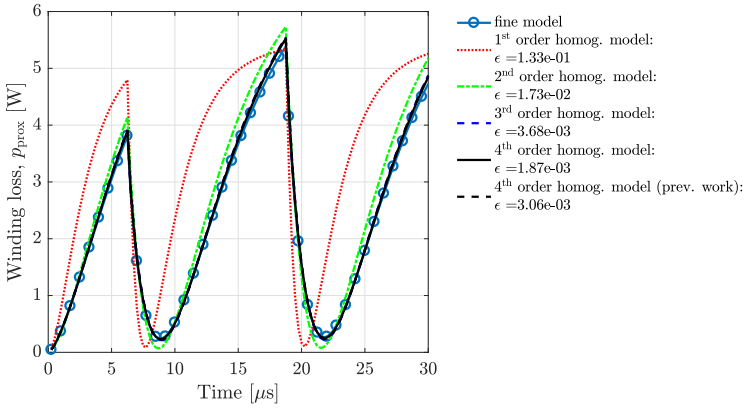

FIGURE 11 Winding loss computed from the fine model and the homogenized model with synthesized networks of different orders, and their normalized RMS errors.

5 | CONCLUSIONS

This paper has proposed an improved method of winding homogenization based on the estimation of a transfer function from frequency-dependent precomputed solutions. Accordingly, a corresponding RL Cauer ladder network is synthesized by the simple Euclidean algorithm for polynomial division. The results evidence the improvement in the accuracy of the winding homogenization compared to the previous work [10] thanks to the well-established RL Cauer ladder network, which eases the transfer-function estimation. To ensure enough accuracy of the estimate for the wide range of frequencies of interest, the transfer function (and the corresponding network) with high orders should be implemented. Based on the implementation with the synthesized 4^{th}-order ladder network, the estimated skin-effect impedance deviates around 6×10^{-3} (vs. 6.6×10^{-3} for the previous work) from the reference solution to the cell problem in the range

of $r/\delta \in [0, 10]$, while the proximity-effect reluctivity deviates only around 6×10^{-5} (vs. 1.67×10^{-3} for the previous work). A 2-D axisymmetric inductor with a nonlinear gapped core is considered as an application example. The number of unknowns in the homogenized model is around 4 times less than its fine-model counterpart even though additional unknowns are introduced in the method. The sparsity of the FE matrices is preserved. Moreover, the magnetic energy in the winding region and winding losses computed from the homogenized model show a good agreement with the ones from the fine model with the relative error of 1.03×10^{-3} and 1.87×10^{-3} respectively. The method is also equally valid in 3-D.

ACKNOWLEDGMENTS

This work was supported by the Walloon Region through WBGreen-FEDO grant 1217703.

APPENDIX: DETERMINING THE NUMBER OF TRIANGULAR ELEMENTS

According to the assumptions in Figure 5 in Section 4.1, the number of triangular elements for the winding region with N conductors (fill factor λ) in the fine model is

$$n_{\text{fine}} = n_{\Delta_\text{r}} + n_{\Delta_\text{i}} + n_{\Delta_{\text{air,insul}}} \tag{23}$$

where n_{Δ_r}, n_{Δ_i} and $n_{\Delta_{\text{air,insul}}}$ are the numbers of triangles in the ring, the inner circle, and the air and insulation respectively. Assuming equilateral triangular mesh with side length $\delta/3$ in the ring region, the first term is

$$n_{\Delta_\text{r}} = \frac{N A_\text{r}}{\Delta_\text{r}} \tag{24}$$

where the area of a triangle Δ_r and the total area A_r are

$$\Delta_\text{r} = \frac{\sqrt{3}}{4}\left(\frac{\delta}{3}\right)^2, \quad A_\text{r} = \pi\left(r^2 - (r-\delta)^2\right). \tag{25}$$

In the inner circle region, assuming equilateral triangular mesh with coarser side length a, the number of triangles in the region is

$$n_{\Delta_\text{i}} = \frac{N A_\text{i}}{\Delta_\text{i}} \tag{26}$$

where the area of a triangle Δ_i and the total area A_i are

$$\Delta_\text{i} = \frac{\sqrt{3}}{4}a^2, \quad A_\text{i} = \pi\,(r-\delta)^2\,. \tag{27}$$

For the mesh of the air and insulation in the winding region, we assume that the side length of the elements is also a leading to the triangular area of Δ_i. This causes the number of elements

$$n_{\Delta_{\text{air,insul}}} = \frac{A_{\text{air,insul}}}{\Delta_\text{i}} \tag{28}$$

with $A_{\text{air,insul}} = \frac{1-\lambda}{\lambda} N\pi r^2$. Substituting (24), (26) and (28) into (23), we obtain

$$n_{\text{fine}} = \frac{N}{\lambda\Delta_\text{i}}\left(\left[1 + \left(\frac{\Delta_\text{i}}{\Delta_\text{r}} - 1\right)\lambda\right] A_\text{r} + A_\text{i}\right). \tag{29}$$

For the homogenized model, the winding region is modeled by a homogeneous rectangular region together with $k \geq 1$ additional basis functions. In contrast to the fine model, the triangular mesh is uniformly generated and each has the side length a (identical to the side length of the element in the air and insulation of the fine model). Thus, the total number of triangular elements in the winding region is

$$\begin{aligned} n_{\text{homog}} &= k\,\frac{A_\text{r} + A_\text{i} + A_{\text{air,insul}}}{\Delta_\text{i}} \\ &= \frac{kN}{\lambda\Delta_\text{i}}\,(A_\text{r} + A_\text{i})\,. \end{aligned} \tag{30}$$

Obviously, if the mesh in the winding regions of both cases are identical and uniform (e.g. at low frequency), leading to $\Delta_\text{i} = \Delta_\text{r}$ or $A_\text{r} = 0$, then $n_{\text{homog}} = k n_{\text{fine}}$ or $n_{\text{homog}} \geq n_{\text{fine}}$. In other words, the homogenized model has no advantages over the brute-force fine model since it yields more unknowns and gives a less accurate solution. In high-frequency eddy-current problems, this rarely occurs because, in practice, the mesh generation in the fine model is considered computationally effective when the mesh around the skin of the conductor is finer than the inner layer or $\Delta_\text{i} > \Delta_\text{r}$.

References

1. Gyselinck J., Dular P.. Frequency-domain homogenization of bundles of wires in 2-D magnetodynamic FE calculations. *IEEE Trans. Magn.*. 2005;41(5):1416–1419.

2. Meunier G., Charmoille V., Guérin C., Labie P., Maréchal Y.. Homogenization for periodical electromagnetic structure: Which formulation?. *IEEE Trans. Magn.*. 2010;46(8):3409–3412.

3. Nan X., Sullivan C. R.. An equivalent complex permeability model for litz-wire windings. *IEEE Trans. Ind. Appl.*. 2009;45(2):854–860.

4. Meeker D. C.. An improved continuum skin and proximity effect model for hexagonally packed wires. *J. Comput. Appl. Math.*. 2012;236(18):4635–4644.

5. Rossmanith H., Albach M., Fischer J., Stadler A.. Improved characterization of the magnetic properties of hexagonally packed wires. *EPE J.*. 2012;22(4):5–10.

6. Igarashi H.. Semi-analytical approach for finite-element analysis of multi-turn coil considering skin and proximity effects. *IEEE Trans. Magn.*. 2017;53(1).

7. Sabariego R. V., Niyomsatian K., Gyselinck J.. Eddy-current-effect homogenization of windings in harmonic-balance finite-element models coupled to nonlinear circuits. *IEEE Trans. Magn.*. 2018;54(3):18–21.

8. Wheeler H.A.. Formulas for the skin effect. In: :412–424; 1942.

9. Gyselinck J, Sabariego R V, Dular P. Time-domain homogenization of windings in 2-D finite element models. *IEEE Trans. Magn.*. 2007;43(4):1297–1300.

10. Sabariego R.V., Dular P., Gyselinck J.. Time-domain homogenization of windings in 3-D finite element models. *IEEE Trans. Magn.*. 2008;44(6):1302–1305.

11. Sato Y., Igarashi H.. Time-domain analysis of soft magnetic composite using equivalent circuit obtained via homogenization. *IEEE Trans. Magn.*. 2017;53(6):2–5.

12. Sato Y., Igarashi H.. Generation of equivalent circuit from finite element model using model order reduction. *IEEE Trans. Magn.*. 2016;52(3):3–6.

13. Kameari A., Ebrahimi H, Sugahara K., Shindo Y., Matsuo T.. Cauer ladder network representation of eddy-current fields for model order reduction using finite element method. *IEEE Trans. Magn.*. 2018;54(3):1–1.

14. Drmac Z., Gugercin S., Beattie C.. Quadrature-based vector fitting for discretized H2 approximation. *SIAM J. Sci. Comput.*. 2015;37(2):A625–A652.

15. Heres P J, Deschrijver D, Schilders W H A, Dhaene T. Combining Krylov subspace methods and identification-based methods for model order reduction. *Int. J. Numer. Model.*. 2007;.

16. Gustavsen B., Semlyen A.. Application of vector fitting to state equation representation of transformers for simulation of electromagnetic transients. *IEEE Trans. Power Deliv.*. 1998;13(3):834–842.

17. Gustavsen B.. Application of vector fitting to high frequency. In: Int. Conf. Power Syst. Transients:1–5; 2003.

18. Sullivan C. R.. Computationally efficient winding loss calculation with multiple windings, arbitrary waveforms, and two-dimensional or three-dimensional field geometry. *IEEE Trans. Power Electron.*. 2001;16(1):142–150.

19. Kotiuga P. R.. Interwinding distributed capacitance and guitar pickup transient response. *IEEE Trans. Magn.*. 2015;51(3):1–4.

20. Dalessandro L., Cavalcante F., Kolar J.. Self-capacitance of high-voltage transformers. *IEEE Trans. Power Electron.*. 2007;22(5):63.

21. De Grève Z., Deblecker O., Lobry J.. Numerical modeling of capacitive effects in HF Multiwinding Transformers—part II: identification using the finite-element method. *IEEE Trans. Magn.*. 2013;49(5):2021–2024.

22. Holmberg P., Bergqvist A., Engdahl G.. Modelling eddy currents and hysteresis in a transformer laminate. *IEEE Trans. Magn.*. 1997;33(2):1306–1309.

23. Valkenburg M.. *Introduction to modern network synthesis*. John Wiley & Sons, Inc.; 1965.

24. Geuzaine C., Remacle J.. Gmsh: A 3-D finite element mesh generator with built-in pre- and post-processing facilities. *Int. J. Numer. Methods Eng.*. 2009;79(11):1309–1331.

25. Dular P, Geuzaine C, Genon A, Legros W. An evolutive software environment for teaching finite element methods in electromagnetism. *IEEE Trans. Magn.*. 1999;35(3):1682–1685.

26. Dular P., Sabariego R. V., Kuo-Peng P.. Three-dimensional finite element modeling of inductive and capacitive effects in micro-coils. *COMPEL - Int. J. Comput. Math. Electr. Electron. Eng.*. 2006;25(3):642–651.